Total Variation-Based Model For Signal Restoration Using Local Meshless Algorithm

Danyal Ahmad*, Mushtaq Ahmad Khan†, Abdul Kabir‡, Muhammad Atif§, Tawab Khan**

Abstract

A noisy signal is transformed into another signal that exhibits fluctuations, called signal fluctuation. This fluctuation is a common challenge in signal processing. In this article, we present a mesh-free Local Meshless Scheme (LMC) for numerically solving the Euler-Lagrange Partial Differential Equation (EL-PDE) associated with the Total Variation (TV)-based model designed to remove additive noise from given data signals. This method employs the Multi-quadric Radial Basis Function (MQ-RBF) as its basis function. The features of this approach effectively eliminate fluctuations from the noisy signals by leveraging meshless applications. Experimental results demonstrate that the proposed LMC exhibits superior performance in terms of Signal to Noise Ratio (SNR) when compared to conventional methods and the Global Meshless Scheme (GMS), across various basis functions. Moreover, the results indicate that the LMCA is faster regarding computation time (CUP time) and requires fewer iterations for convergence than both the conventional method and the GMS.

Keywords: Euler Lagrange Partial Differential Equation; Additive Noise; Total Variation-Regularization; Signal to Noise Ratio; Radial Basis Function Interpolation; Multi-quadric Radial Basis Function; Local Meshless Scheme; Global Meshless Scheme.

Introduction

Signal processing is a field of engineering and computer vision that focuses on modifying analyzing, and synthesizing signals. Signals can be any spatial-varying or time-varying quantity such as audio signals, images, or sensor data. The main goals of signal processing are to extract useful information, improve signal quality, and transform signals into a more desirable form. Signal processing techniques are applied in various fields, including telecommunications, audio and video processing, speech recognition, and control systems. Over the past few decades, a lot of research has been done on signal denoising, an inverse problem and a

*Department of Natural Sciences and Humanities, University of Engineering and Technology Mardan, Mardan 23200, Pakistan, tajbakht0@gmail.com

† Corresponding Author: Department of Natural Sciences and Humanities, University of Engineering and Technology Mardan, Mardan 23200, Pakistan, mushtaq@uetmardan.edu.pk

‡Department of Natural Sciences and Humanities, University of Engineering and Technology Mardan, Mardan 23200, Pakistan, kabirabdul5008@gmail.com

§Department of Natural Sciences and Humanities, University of Engineering and Technology Mardan, Mardan 23200, Pakistan, atifkhilji1122@gmail.com

**Department of Natural Sciences and Humanities, University of Engineering and Technology Mardan, Mardan 23200, Pakistan, tawabkhan213@gmail.com

highly functional field in image processing and computer vision. In this article, we consider a model for removing additive noise, although there are various types of noises. This can be modeled as under.

$$v_0 = v + \eta, \quad (1)$$

Where v_0 represents the provided noisy signal with additive noise η, and v is called true signal, all are expressed on the domain $\Omega \in R.^2$

Various researchers have proposed various useful numerical approaches that have been used to address models related to signal denoising associated with additive noise, such as stochastic methods, wavelet approaches, and anisotropic diffusion techniques (Li et al., 2018; Satapathy et al., 2019; Naveed et al., 2019; Kervrann, 2004; Polzehl & Tabelow, 2007; Ramadhan et al., 2017; Luo et al., 2019; Bai & Feng, 2018). Recently, TV-based models for image restoration have been used as PDE-based tools, resulting in many successful restoration outcomes for images and signals (Krishnanetb al., 2006; Rudin & Osher, 1994; Rudin et al.,1992). Rudin et al. (1992) have proposed the first TV-based model for signal and image restoration having additive noise.

Regardless of the inherent effects of TV regularization, the Rudian, Osher and Fatemi (ROF) model efficiently eliminates signal and image noise while maintaining image edges (Chan et al., 2006; Osher et al., 2005). However, because of its non-linearity and non-differentiability characteristics, it also shows certain undesired consequences, like signal contrast denoising and time computation Rudin et al., 1992; Osher et al., 2005; Chang et al., 2009; Lysaker et al., 2004 ; Lysaker et al., 2003). Rudin et al. (1992) have introduced an artificial time-marching procedure for the connected EL-PDE. The TV method involves progressively reducing the pixel values in a signal without compromising the resolution. The TV-based methods are best suited for signals with regions that are piecewise constant. During the iterations, the signal noise is reduced, and if the iterations are not stopped, a constant-valued signal is eventually obtained. Thus, in TV based approach we need stopping measures to control the over-smoothing of the noisy signal. A few good features of the ROF model provide us with a smooth solution for the restoration of signals that contain additive noise (Clason et al., 2010). However, this model has several flaws because of the non-linearity and non-differentiability of the related PDE, which leads to signal problems. However, there is always potential for development. To minimize these problems, we therefore modify the mesh-free RBF collocation approach in our work.

In the 1970s, RBF-based methods were formulated to control the structural conditions of existing numerical schemes. These processes are suitable for dispersed data sources (Jiang et al., 2015). Therefore, rather than using a numerical technique, the application may determine the

domain's shape. In recent years, RBF techniques have grown significantly in both approximation theory and PDEs numerical solution. The RBF interpolation process, sometimes referred to as the Collocation methods, is the most frequently utilized RBF approach for these types of problems (Kansa, 1990a; Kansa, 1990b; Kansa, 1999). The meshless properties of RBF schemes keep these schemes best because they need a set of points that are required to discretize the continuous domain. RBF approaches have proven to be more efficient than. RBF techniques have demonstrated superior efficiency compared to FDM (Kansa,1999; Jankowska at al., 2018; Zerroukat et al., 1998). Pseudo-spectral method (Larsson & Fornberg, 2003; Li at al., 2003). The RBF methods are domain-specific strategies with various features, such as the finite element approach for approximating the solution of nonlinear equations. See (Jankowska at al., 2018; Parand & Rad, 2012; Ordokhani & Razzaghi 2008; Houstis, 1978; Eslahchi at al., 2014; Doha et al., 2013). For further details on RBF collocation techniques. RBF techniques can be used both Globally and Locally. Corresponding to other traditional techniques, the Global Meshless Method can efficiently solve PDEs for a smooth solution due to its adaptive properties and computational approach. The Global Meshless Method has a primary disadvantage in its global structure-property, leading to the use of full matrices in Global Meshless Scheme due to PDEs discretization, resulting in constant ill conditions (Kansa, 1990) which sometimes produces issues in smooth solution in PDEs. To address the sensitivity of the shape parameter and the ill-conditioning of the Global Meshless Scheme, a new approach known as the LMS has been developed. This technique was originally presented in (Sarra, 2011). For diffusion problems. It showed improvements in accuracy and efficiency due to its local structure property, efficient computational approach, and adaptive property (Chenoweth, 2012; Hosseini & Hashemi, 2011). The LMS approach has been broadly applied to different engineering and science situations due to its convenience (Sarra, 2012; Shen, 2011). The LMS method aims to reduce the dimension of the collocation matrix by solving multiple small matrices that collocate the overlapping sub-domains of influence. Each small matrix has a size equal to the number of points within the influence domain of each point. This method has also the application of locally adaptive nature and computational efficiency and easy mathematical implementation. Motivated by the applications of the LMS, we apply the LMS for the approximate solution of EL-PDE connected with the ROF model for additive noise removal from signals. This meshless scheme will effectively remove the noise from the noisy signal and will take less time due to its above-mentioned applications.

The paper is arranged as follows: The second part presents the relevant work. The first subpart consists of the ROF model for signal denoising, whereas the second subpart contains RBF interpolation. The third part explores the mesh-based gradient descent numerical approach for solving EL-PDE with the ROF model. This section also includes a proposed meshless approach LMS for numerically solving EL-PDE connected with the ROF model. The fourth part explains the experimental results. Finally, the final part provides the paper's conclusions. The appendix is presented at the end of this article.

Related Work

Total Variation (TV) Based ROF model

Digital image processing employs TV (Total Variation) regularization to effectively reduce noise in images and signals. This technique is also essential for addressing inverse problems and performing numerical computations. Regularization is particularly valuable because it preserves edges while eliminating excessively noisy frequencies from both images and signals. Additionally, it is convex. The TV of an image $v(x,y) = \Omega \to \Re^2$ is defined as follows:

$$TV(v) = \int_{\Omega} |\nabla v| \, dxdy \quad where \quad |\nabla v| = \sqrt{v_x^2 + v_y^2}. \tag{2}$$

The first TV-based model for denoising data from noisy signals impacted by additive noise was presented by Rudin et al. (ROF). They employed total variation (TV) regularization as a technique for this process. Their methodology yielded significant restoration results. The TV regularization method offers a minimization technique for the model presented in Equation (1).

$$\min_{v}\{E(v)\} = \min_{v} \int_{\Omega} |\nabla v(x,y)| \, d\Omega + \lambda \int_{\Omega} (v - v_0)^2 \, d\Omega, \tag{3}$$

Where $|\nabla v| = \sqrt{v_x^2 + v_y^2}$.

The first term refers to the TV regularization of $E(v)$ while the subsequent term indicates the data fitting component. The parmeter λ is the regularization parameter and is used to strike a balance between the denoising and smoothing of the denoised signal, which is usually affected by the amount of noise present. The EL-PDE connected with ROF model is provided in the following from.

$$-\nabla\left[\frac{\nabla v}{|\nabla v|^2 + \varepsilon}\right] + 2\lambda(v - v_0) = 0 \; in \; \Omega \; for \; \epsilon > 0, (x,y) \in \Re, \tag{4}$$

or

$$-\frac{\partial}{\partial x}\left(\frac{v_x}{\sqrt{v_x^2+v_y^2}}\right)+\frac{\partial}{\partial y}\left(\frac{v_y}{\sqrt{v_x^2+v_y^2}}\right)+2\lambda(v-v_0)=0\ in\ \Omega, \quad (5)$$

with $\frac{\partial v}{\partial n}=0$ on the boundary of $\Omega=\partial\Omega$. The time-dependent EL-PDE of Equation (5) is presented as under.

$$v_t=\nabla\left[\frac{\nabla v}{|\nabla v|^2+\varepsilon}\right]+2\lambda(v-v_0)\ \ in\ \Omega\ for\ \ t>0,(x,y)\in\Re, \quad (6)$$

or

$$\frac{\partial v}{\partial t}=\frac{\partial}{\partial x}\left(\frac{v_x}{\sqrt{v_x^2+v_y^2}}\right)+\frac{\partial}{\partial y}\left(\frac{v_y}{\sqrt{v_x^2+v_y^2}}\right)+2\lambda(v-v_0)=0, \quad (7)$$

in $\Omega\ for\ t>0,(x,y)\in\Re$.

For the given $v(x,y,0)$ and also $\frac{\partial v}{\partial n}=0$ on $\partial\Omega$. For further information, see Chambolle et al., (2010).

Radial Basis Function Interpolation

Let us discuss the RBF approach (Khan et al., 2017). RBF is a real-valued function whose value depends only on the distance from the origin, so that $\varphi(x)=\varphi(\|x\|)$, or alternatively on the distance from some other point c, called center so that $\left(\varphi(x,c)=\varphi(\|x-c\|)\right)$. Any function that satisfies the property $\varphi(x)=\varphi(\|x\|)$ is called the radial basis function. Radial Basis functions are Gaussian functions, multi-quadric functions and inverse multi-quadric functions. RBF method monographs (Shan et al., 2009) generally contain information on RBF methods. For specific data points or evaluation points $\{x_i,T_i\}_{i=1}^{N}$, local RBF is equivalent to the global RBF approach. The global RBF approach allows us to freely choose the center points, which is the only difference. However, choosing the center locations is restricted when using the local RBF approach. To do this, we require the stencil value and one evaluation point, which is used to measure the center values (Micchelli, 1984). But for $\left\{x_{i,j},T_{i,j}\right\}_{j=1}^{M}$ Center points and evaluation points.

$$v(x)=\sum_{i=1}^{N}P_i\varphi\left(\left\|x-x_j^c\right\|_2\right), \quad (8)$$

Which results in $B=\left[\varphi_{ij}\right]=\left(B_{ij}\right)\in R^{M\times M}$ as given below:

$$B = \begin{bmatrix} \varphi(\|x_1^c - x_1^c\|_2), \varphi(\|x_1^c - x_2^c\|_2) \cdots \varphi(\|x_1^c - x_M^c\|_2) \\ \varphi(\|x_2^c - x_1^c\|_2), \varphi(\|x_2^c - x_2^c\|_2) \cdots \varphi(\|x_2^c - x_M^c\|_2) \\ \vdots \\ \varphi(\|x_M^c - x_1^c\|_2), \varphi(\|x_M^c - x_2^c\|_2) \cdots \varphi(\|x_M^c - x_M^c\|_2) \end{bmatrix}, \quad (9)$$

Where $P = (P_1, P_2, \dots, P_n)^t$, $\omega_o = \left(\omega_o(x_1), \omega_o(x_2), \dots, \omega_o(x_n)\right)^t$, are unknown (to be determined) and known matrices of orders $M \times 1$. So Equation (8) can be rewritten as under.

$$\begin{bmatrix} \varphi(\|x_1^c - x_1^c\|_2), \varphi(\|x_1^c - x_2^c\|_2) \cdots \varphi(\|x_1^c - x_M^c\|_2) \\ \varphi(\|x_2^c - x_1^c\|_2), \varphi(\|x_2^c - x_2^c\|_2) \cdots \varphi(\|x_2^c - x_M^c\|_2) \\ \vdots \\ \varphi(\|x_M^c - x_1^c\|_2), \varphi(\|x_M^c - x_2^c\|_2) \cdots \varphi(\|x_M^c - x_M^c\|_2) \end{bmatrix} \begin{bmatrix} P_1 \\ P_2 \\ \vdots \\ P_N \end{bmatrix} = \begin{bmatrix} \omega_o(x_1) \\ \omega_o(x_2) \\ \vdots \\ \omega_o(x_N) \end{bmatrix}. \quad (10)$$

Equation (10) can be rewritten as under.

$$BP = \omega_0, \quad (11)$$

Where$B$ is called $M \times M$ system matrix So Equation (11) can be written as under.

$$P = B^{-1}\omega_o \quad (12)$$

The invertible matrix B (non-singular matrix) depends upon the basis function used in RBF used in B. Now for $\left\{x_j^c, \omega_{0_j^o}\right\}_{j=1}^{M}$ stencil points and $\left\{x_i, \omega_{0_j^o}\right\}_{i=1}^{N}$ evaluation points. The interpolation condition is for

$$V(x) = \sum_{i=1}^{N} P_j \, \varphi\left(\left\|x_i - x_j^c\right\|_2\right) = \omega_{o_i} \quad (13)$$

$i = 1,2,3 \dots N \; j = 1,2,3 \dots M$ and $M < N$.

So (13) results in the following system of equations.

$$KP = \omega_o. \quad (14)$$

Here $K = [k_{i,j}] = \left[\phi\left(\left\|x_i - x_j^c\right\|_2\right)\right]$ for $i = 1,2,3,\dots,N$ and $j = 1,2,3,\dots,M$and is defined in given matrix form.

$$K = \begin{bmatrix} \varphi(\|x_1 - x_1^c\|_2), \varphi(\|x_1 - x_2^c\|_2) \cdots \varphi(\|x_1 - x_M^c\|_2) \\ \varphi(\|x_2 - x_1^c\|_2), \varphi(\|x_2 - x_2^c\|_2) \cdots \varphi(\|x_2 - x_M^c\|_2) \\ \vdots \\ \varphi(\|x_N - x_1^c\|_2), \varphi(\|x_N - x_2^c\|_2) \cdots \varphi(\|x_N - x_M^c\|_2) \end{bmatrix} \quad (15)$$

with $N \times M$ order matrix is called an evaluation matrix. Also $P = (P_1, P_2, P_3, \dots, P_M)^t$and $\omega_o = \left(\omega_o(x_1), \omega_o(x_2), \omega_o(x_3), \dots, \omega_o(x_n)\right)^t$.

So

$$\omega_o = KP. \quad (16)$$

Put the value of P from Equation (12) in Equation (16), we have

$$\omega_{approx} = KB^{-1}\omega_o. \quad (17)$$

Let

$$KB^{-1} = E. \quad (18)$$

Then Equation (17) implies that

$$\omega_{approx} = E\omega_o. \quad (19)$$

Equation (19) $N \times 1$ system and is called the approximation solution of the function ω. for more information, see (Khan et al., 2017).

Numerical Schemes for Solution of ROF Model

Traditional approach for ROF Model (M1)

The ROF model is defined as a constrained optimization problem presented in Equation (8).

$$\min_v\{E(v)\} = \min_v \int_\Omega |\nabla v(x,y)|\, d\Omega + \lambda \int_\Omega (v - v_0)^2\, d\Omega. \quad (20)$$

Here v_0 is provided degraded signal, v represents the denoised signal and λ is a regularization parameter, a constant that determines the tradeoff between two terms. The denoised signal v is seen utilizing given approach.

$$v_{ij}^{k+j} = v_{ij}^k + \frac{\Delta\tau}{\hbar}\left[\nabla_x^- \left(\frac{\nabla_x^- v_{ij}^k}{\sqrt{\left(\nabla_x^+ v_{ij}^k\right)^2 + \left(m_1\left(\nabla_y^+ v_{ij}^k\right), \left(\nabla_y^- v_{ij}^k\right)^2\right)}}\right) + \left(\nabla_y^- \frac{\nabla_y^- v_{ij}^k}{\sqrt{\left(\nabla_y^+ v_{ij}^k\right)^2 + \left(m_2\left(\nabla_x^+ v_{ij}^k\right), \left(\nabla_x^- v_{ij}^k\right)^2\right)}}\right)\right] - \Delta\tau\lambda\left(v_{ij}^k - z^0(i\hbar, j\hbar)\right). \quad (21)$$

For $= 1, 2, \ldots, m_1$, $j = 1,2, \ldots, m_2$ with boundary conditions $v_{0j} = v_{1j}$, $v_{m_1 j} = v_{m_1-1 j}$, $v_{i0} = v_{im_2} = v_{im_2-1}$. Where

$$\nabla_x^{\pm} = \pm\left[v_{i\pm1,j} - v_{i,j}\right], \quad \nabla_y^{\pm} = \pm\left[v_{i,j\pm1} - v_{i,j}\right], \quad (22)$$

$$\left|\nabla_x\left(v_{i,j}\right)\right|_\epsilon = \sqrt{\nabla_x^+ + \left(v_{i,j}\right)^2 + \left(m_1\left[v_y^+\left(v_{i,j}, \nabla_y^- v_{i,j}\right)\right]\right)^2 + \epsilon}, \quad (23)$$

$$\left|\nabla_y\left(v_{i,j}\right)\right|_\epsilon = \sqrt{\nabla_y^+ + \left(v_{i,j}\right)^2 + \left(m_1\left[v_x^+\left(v_{i,j}, \nabla_x^- v_{i,j}\right)\right]\right)^2 + \epsilon}, \quad (24)$$

with $m[\alpha, \beta] = \left(\frac{sign(\alpha)+sign(\beta)}{2}\right).min(|\alpha|, |\beta)|$. For more details, see Rudin et al. (1992).

Proposed Local Meshless Scheme (M2)

In this section, we apply the LMC on EL-PDE connected with ROF to overcome associated the difficulties with EL-PDE and to obtain a smooth solution concerning signal restoration. Assume that $\{x_i\}_{i=1}^N$ is the

N different data points on the domain $\Omega \subseteq R^2$. Thus, the following equation corresponds to for every RBF,$\varphi(r) = \|r\|_2 in R^2$i.e. $r = (x, y)$. For$\{xc_j\}_{j=1}^{N_c}$, given N_c centers, the RBF can be written without the demand for a polynomial representation.

$$v(x) = \sum_{i=1}^{N_C} p_j \varphi\left(\left\|x - xc_j\right\|_2\right), \text{ for i, j=1,2,3 ,...,N}_c. \quad (25)$$

Here $p_j$is coefficient in RBF and can be defined as under.

$$S(x_i) = v_0, \quad (26)$$

a collection of points that frequently line up with centers.

$$Hp = v_0, \quad (27)$$

Where $p = \left(p_1, p_2, p_3 \ldots . p_{N_C}\right)^t$ is unknown and $v_0 = \left(v_{01}, v_{02}, v_{03}, \ldots \ldots v_{0N_c}\right)^t$ is known are $N_C \times 1$ matrices.The interpolation matrix, or matrix H, is provided by

$$H = [\varphi_{ij}] = \left[\left(\left\|x_i - xc_j\right\|_2\right)\right]_{1 \le i,j \le N_C}. \quad (28)$$

Since this system matrix H is always a positive definite matrix, it is $N_c \times N_c$ square and always invertible (Levesley, 2004; Madych & Nelson, 1983; Jiang & Zhang 2013). Consequently we obtain:

$$p = H^{-1} v_0, \quad (29)$$

Again, Equation (25) is used to estimate the interplant at N inspection points $\left(\{x_i\}_{i=1}^{N}\right)$ by producing the $N \times N_c$evaluation matrix$K$, which is provided below.

$$K = [\varphi_{ij}] = \left[\varphi\left(\left\|x_i - xc_j\right\|_2\right)\right] for i = 1,2,\ldots Nj = 1,2,\ldots . N_c,$$

$$v = Kv_0. \quad (30)$$

Now, from Equation (29) and Equation (30), the following Equation is obtained.

$$v = KH^{-1} v_0,$$

or

$$v = Mv_0, \quad \text{where} \quad M = KH^{-1}, \quad (31)$$

Where, when v is a matrix of rank$N_c \times 1$., provides an approximate solution at any point in Ω.

The time-dependent PDE from the ROF model Equation (7) is redefined as given.

$$\frac{dv}{dt} = \frac{(v_{xx}+v_{yy})(v_x^2+v_y^2)-(2v_x v_y v_{xy}+v_x^2 v_{xx}+v_y^2 v_{yy})}{(v_x^2+v_y^2)^{\frac{3}{2}}} + 2\lambda(v - v_0). \quad (32)$$

The implicit gradient decent procedure is then used on the Equation (32) and thus we acquire the subsequent equation.

$$\frac{v^{(n+1)}-v^{(n)}}{dt} = \frac{\left(v_{xx}^{(n)}+v_{yy}^{(n)}\right)\left((v_x^2)^{(n)}+(v_y^2)^{(n)}\right)-\left(2v_x^{(n)}v_y^{(n)}\left(v_x^{(n)}v_y+v_xv_y^{(n)}\right)+v_x^2v_{xx}^{(n)}+v_y^2v_{yy}^{(n)}\right)}{\left((v_x^2)^{(n)}+(v_y^2)^{(n)}\right)^{\frac{3}{2}}} - 2\lambda(v^{(n)})(v^{(n)}-v_0^0). \quad (33)$$

We apply Equation (31) in Equation (33) which result in nonlinear system of Equations which is solved by the LMC. The Gauss–Jacobi iterative algorithm is employed on the LMC based resultant system equations which is written as under.

$$G\left(v^{(n)}\right)v^{(n+1)} = G\left(v^{(n)}\right)v^{(n)} + dt\left[\left(v_{xx}^{(n)}+v_{yy}^{(n)}\right)\left((v_x^2)^{(n)}+(v_y^2)^{(n)}\right)-\left(2v_x^{(n)}v_y^{(n)}\left(v_x^{(n)}v_y+v_xv_y^{(n)}\right)+v_x^2v_{xx}^{(n)}+v_y^2v_{yy}^{(n)}\right)\right] - G\left(v^{(n)}\right)dt\left[2\lambda\left(v^{(n)}\right)\left(v^{(n)}-v_0^0\right)\right], \quad (34)$$

where $G(v)=\left(v_x^2+v_y^2\right)^{\frac{3}{2}}, v_x=\omega_x v_0, v=\omega_y v_0, v_{xx}=\omega_{xx}v_0, v_{yy}=\omega_{yy}v_0, \frac{\partial v}{\partial n}=v_n=\omega_n v_0, v_0^0=v_0.$

The suggested LMC M2 allows for more flexibility in selecting an RBF, as it does not always need to satisfy Equation (34). The most widely used RBF in collocation methods is Multi-Quadric (MQ). The MQ-RBF (Jiang & Zhang 2013; Guo et al., 2016) can provide accurate spectral results with the right shape parameter c. The shape parameter c in RBF recreates a crucial role in the smoothness of our method M2. Our proposed methodology LMCA improves the accuracy and smoothness of signal denoising with additive noise when c is optimal. This LMC M2 approach adjusts the parameters c and λ involved based on the signal size and noise level. Here, "head and trail" method is used to select the optimal values of parameters involved.

Algorithm 1:

RBF Interpolation:

1. Let N_c be the center pixel points and let N be the total number of n pixel points that are employed with stencil points n_1 surrounding the center point xc_n in the RBF approximation process.
2. Compute p using MQ-RBF and Equation (29).
3. Utilizing Equation (31) through MQ-RBF, calculate$v$.

TV Regularization:

4. Decide on the weights for $\varepsilon, h, dt, \lambda,$ and v_0.
5. Introduce $n$as N_c number of data pixel centers i.e., $xc_1 \le xc_2 \le \ldots\ldots xc_n$, next pick $n=0$.
6. Substitute MQ-RBF utilizing Equation (31) in Equation (34).

7. Select $n = n + 1$ for every data center point xc_i for$1 \le i \le N$, and then use LMC with $v_0^0 = v_0$ to calculate $v^{(n+1)}$ in accordance with Equation (34).
8. $\frac{\|v^{(n+1)} - v^{(n)}\|}{\|v^{(n)}\|} \le \varepsilon = 10^{-5}$ Procedure is employed to stop the iterative method and proceed to Step (10).
9. Go back to step (7).
10. End.
11. Result $v = v^{(n+1)}$.

Results and Discussion

This section includes experimental results and an analysis of the suggested scheme, LMC M2 performance. Signals are utilized to evaluate the M1 and M2 methods' performance. In this work, our focus is on signal denoised with additive Gaussian noise (mean $p = 0$, varianceL_1) and salt and pepper noise (mean $p = 0$, variance L_2). To verify the signal restoration outcomes of the suggested LMC M2 and compare them to the traditional mesh-based approach M1. We choose a signal size with xc_i, and apply the suggested meshless approach M2.signal-to-noise ratio (SNR) is taken into consideration to quantify the denoised signal. This measure is widely used to evaluate the quality of the restored signal. SNR is calculated as.

$$SNR = 10 \times log_{10} \frac{\|v - v_0\|}{\|n - n_0\|}, \quad (35)$$

Where B is the final denoised image, $M \times N$ denotes the image data size, and H is the original image that is provided. The greater the SNR value to better the restoration result. The suggested scheme M2 faster convergence achievement and the stoppage of the iterative procedure are represented by the following formula.

$$\frac{\left\|v^{(n+1)} - v^{(n)}\right\|}{\left\|v^{(n)}\right\|} \le \varepsilon, \quad (36)$$

Where ε shows the highest permitted error. Here, it is set to be 10^{-4}. In this section the outcomes of techniques M1 and M2 are tested and compared using the Multi-quadric (MQ) RBF. For each point(x_i, y_j), Multi-quadric (MQ) RBF is expressed in the downward equation.

$$\phi_j(x, y) = \sqrt{c^2 + r_j^2} = \sqrt{c^2 + \left(\left(x - x_j\right)^2 + \left(y - y_j\right)^2\right)}, \quad (37)$$

Where $r_j^2 = (x - x_i)^2 + (y - y_j)^2$.

Also, for every selected point (x_i, y_j) has the following IMQ-RBF expression:

$$\phi_j(x,y) = \left(\frac{1}{\sqrt{c^2 + \left((x-x_i)^2 + (y-y_j)^2\right)}} \right) \tag{38}$$

Similarly, for every selected point (x_i, y_j) has the following Gaussian expression:

$$\phi_j(x,y) = \left((e)^{-c^2\,(x-x_i)^2+(y-y_j)^2}\right) \tag{39}$$

Experiment 1

This test compares the implementation of two distinct noise removal techniques, M1 and M2, for restoring signals deteriorated by additive Gaussian noise and Salt and Pepper noise with noise levels of $L_1 = 27\%$ and $L_2 = 32\%$, respectively. These actual and degraded signals are given in Figures 1(a), 1(b), 1(c), and 1(d), respectively. The signal reformed signals using M1 and M2 are shown in Figures 1(e), 1(f), 1(g), and 1(f), respectively, for comparison. Although M1 repaired the signal, the LE-PDE connected with the additive and salt and pepper noises removal model in the mesh-based method led to nonlinearity and non-differentiability, resulting in insufficient restoration outcomes despite the use of TV regularization. These results are shown in Figures 1(e) and 1(f). On the other hand, M2, which utilizes local meshless applications, localization, adaptive natures, and MQ-RBF, delivered excellent signal rehabilitation effects compared to M1, as illustrated in Figures 1(g) and 1(h). Here we take center through the localized method are 80 points. Further, Table 1 demonstrates that the signal-to-noise ratio (SNR) values of M2 are greater than those of M1, indicating the superior signal restoration performance of M2 over M1. Furthermore, M2 required fewer iterations and less CPU time to converge than M1, indicating its quicker restoration performance due to computational efficiency and easy mathematical implementation which are given in Table 2.

Table 1: SNR values comparison between M1 and M2.

S.No.	Signal selected from the Image	Size	M1	M2
			SNR	SNR
1	110^{th}	512	23.71	24.08
2	150^{th}	512	24.29	24.73

Table 2: M1 and M2 comparison regarding the number of iterations and time in seconds required for convergence.

S.No.	Signal taken from the Image	Size	M1		M2	
			Iter	Time(s)	Iter	Time(s)
1	110^{th}	512	14	5.05	10	4.06
2	150^{th}	512	19	8.59	11	5.22

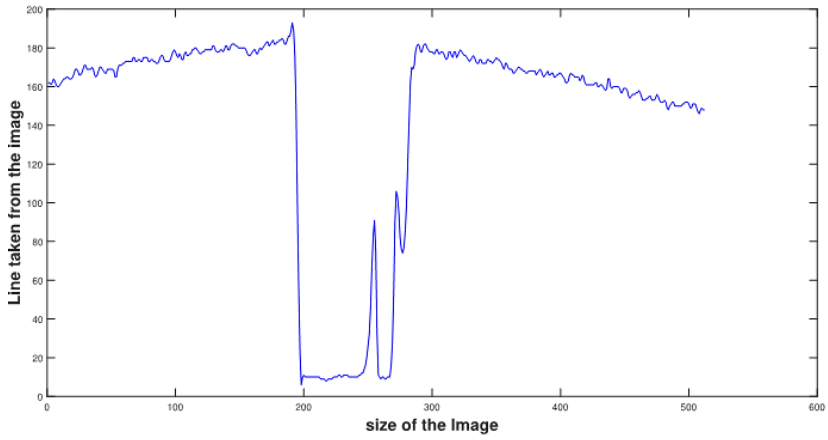

(a) True signal

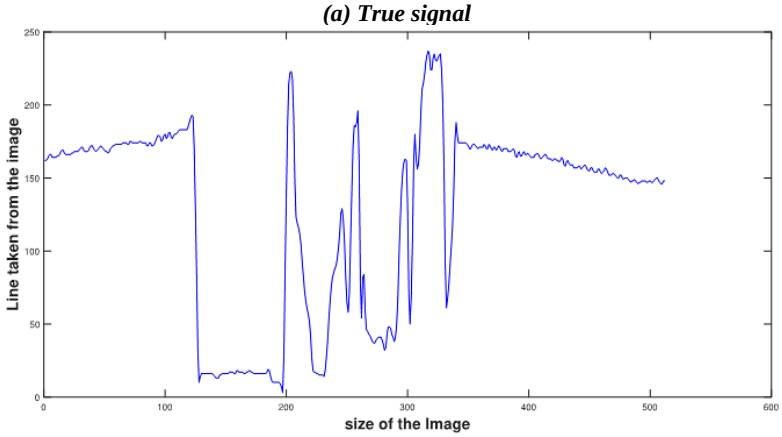

(b) True signal

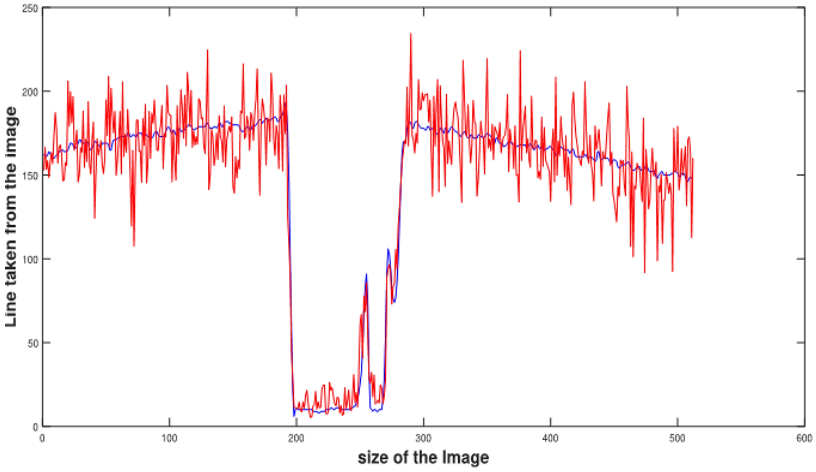

(c) True and noise signals

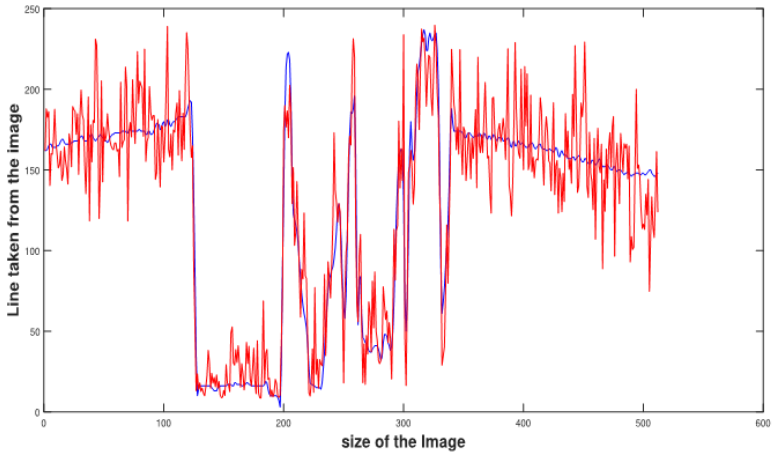

(d) True and noise signals

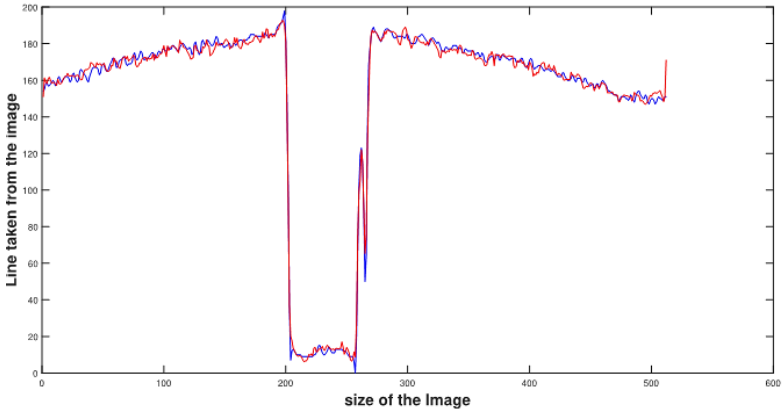

(e) M1

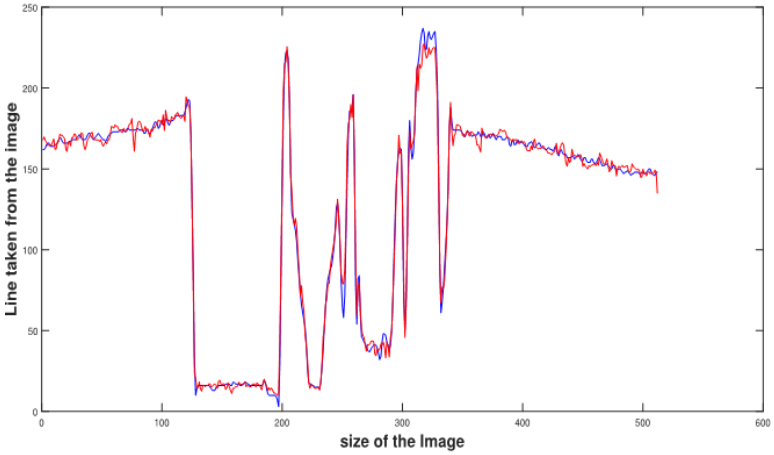

(f) M1

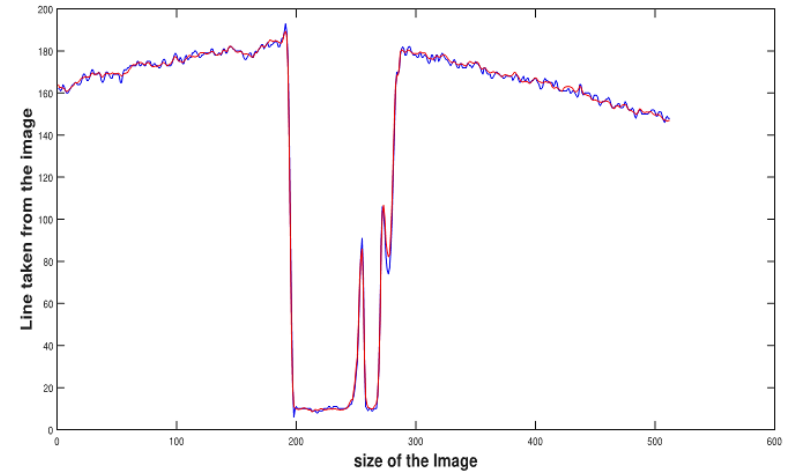

(g) M2

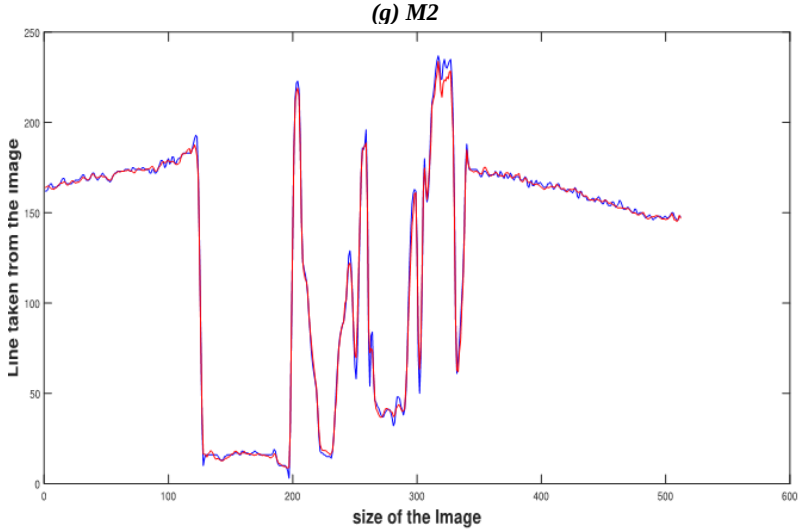

(h) M2

Figure 1 Signals (a) and (b) show 110th and 150th original signals taken from an image, (c) and (d) represent the original and noisy signals having additive Gaussian noise $L1 = 27\%$ and salt and pepper noise $L2 = 32\%$, respectively; (e) and (f) indicate the original and denoised signals using M1; (g) and (h) represent the de-noised signals using LMCA M2 with $c = 1.21$ and $\lambda = 10$. Here the blue line indicates the original signal while the red line indicates the noisy or restored signal.

Experiment 2

In this investigation, we experimented with M1 and M2 for signal restoration using both the actual signal and a noisy signal with $L_1 = 34\%$ additive Gaussian noise. The signals are illustrated in Figures 2(a) and

2(b). M1 did not perform well in signal restoration due to the mesh-based solution of nonlinear and non-differentiable EL- PDE associated with the model, as displayed in Figure 2(c). On the other hand, the proposed meshless strategy M2 was tested with the same shape parameter c=1.17 but for two different center points, p=150 and p=200. It was observed that selecting more center points resulted in better restoration performance than selecting fewer center points. In both cases, the signal restoration results by M2 were superior to M1 due to its meshless application mentioned in test 1, as presented in Figures 2(d) and 2(e). Table 3 indicates that the SNR values of M2 are greater than the M1 value, demonstrating the superior signal restoration performance of M2 over M1. The SNR values were also greater for center values p=200 than center values p=150 for M2 for the same shape parameter, showing better restoration performance with a greater number of center points. Additionally, Table 4 shows that the number of iterations and CPU time required for convergence of M2 is less than M1, representing the faster image restoration of M2 over M1 due to the meshless applications discussed in experiment 1. Moreover, the number of iterations and CPU time of M2 for higher values of centers p=200 are less than the lower values of centers p=150 for the same shape parameter, highlighting the quicker signal restoration performance of M2 for higher values of centers than lower values of centers.

Table 3: Representation of SNR values of M1 and M2 for image restoration.

S. No.	Signal chosen of the Image	Size	M1	M2	
			SNR	SNR(p=150)	SNR(p=200)
1	220^{th}	512	24.01	24.67	24.87

Table 4: Comparison of M1 and M2 regarding number of iterations and CPU times in seconds.

S.No.	Signal taken from the Image	Size	M1		M2			
					P=150		p=200	
			Iter	Time(s)	Iter	Time(s)	Iter	Time(s)
11	220^{th}	512	20	17.7	14	12.9	9	8.22

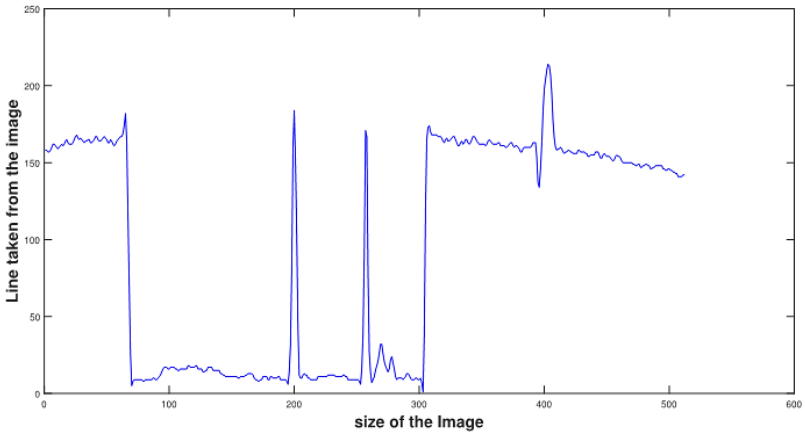

(a) True signal

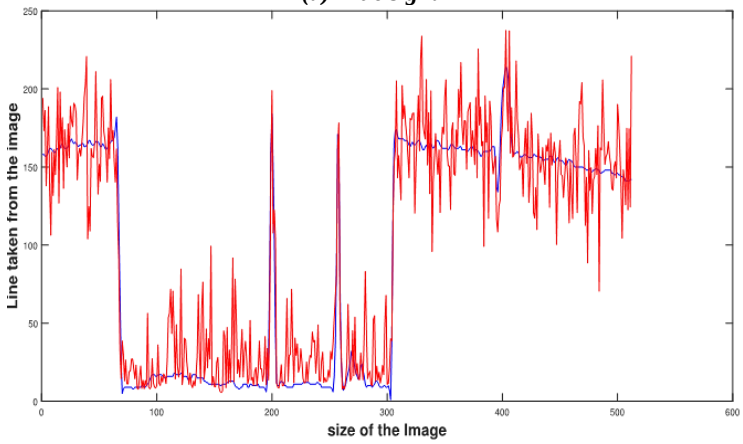

(b) True and noise signals

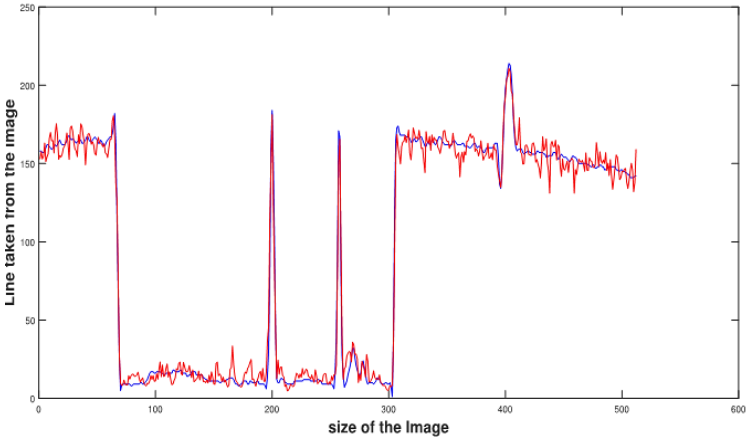

(c) M1

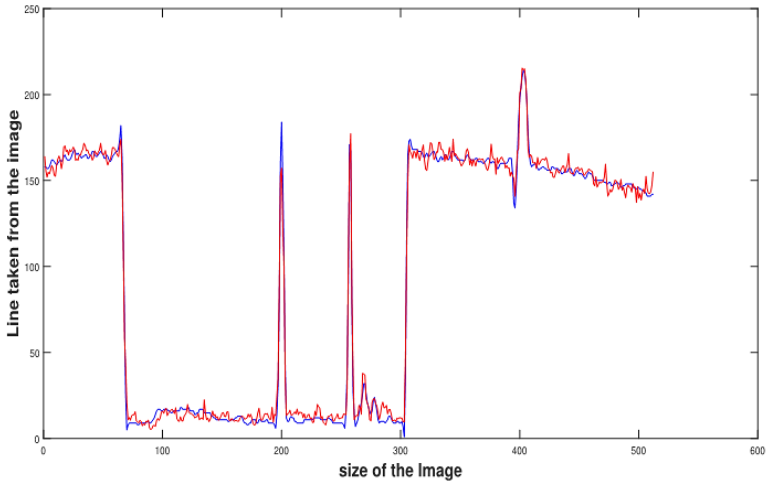

(d) M2 with p= 150

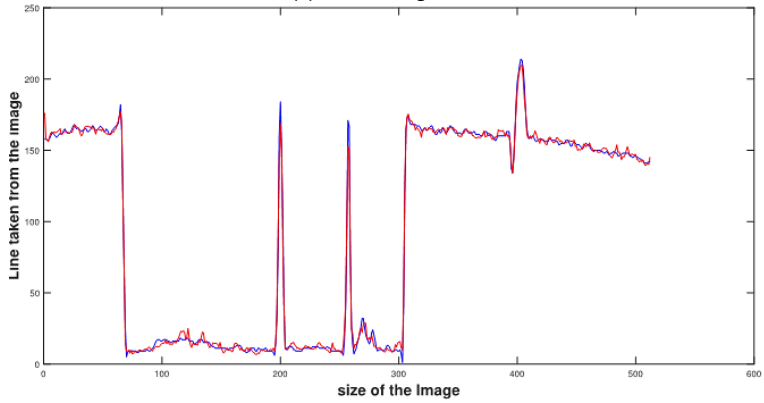

(e) M2 with p= 200

Figure 2: (a) shows the 300th original signal taken from Lena image; (b) indicates the original and noisy signal connected to additive Gaussian noise $L1 = 34\%$; (c) shows the original and restored signals by M1; while (d) and (e) represent the original and restored signals by M2 connected with centers$p = 150$and$p = 200$, respectively. In this case, the red line represents the noisy or restored signal, and the blue line represents the original signal. The parameter values are $c = 1.16$and $\lambda = 13$.

Experiment 3

In this analysis, M2 is compared with M1 for signal restoration from noisy signals with Salt and Pepper noise at a noisy level of $L2 = 38\%$. The real and noisy signals are shown in Figures 3(a) and 3(b). M2 displayed better and quicker restoration performance than M1 due to the meshless application used in M2 over M1. These signals are shown in Figures 3(c), 3(d), 3(e), 3(f), and Table 5, respectively. Additionally, the

suggested meshless approach M2 experiments on three different basis functions: IMQ-RBF, GA-RBF, and MQ-RBF for signal restoration. The study found that the signal restoration results achieved using MQ-RBF were better than those obtained using the other two basis functions, IMQ-RBF and GS-RBF, as reported in [20]. Additionally, the results produced by GA-RBF were superior to those of IMQ-RBF for M2. These findings are illustrated in Figures 3(d), 3(e), 3(f), and Table 5, respectively.

Table 5: Comparison of SNR values of M1 and M2 which is connected with IMQ-RBF, GS-RBF, and MQ-RBF, respectively.

S.No.	Signal selected of the Image	Size	SNR			
			M1	M2(IMQ)	M2(GA)	M2(MQ)
1	320th	512	24.19	24.70	24.87	25.13

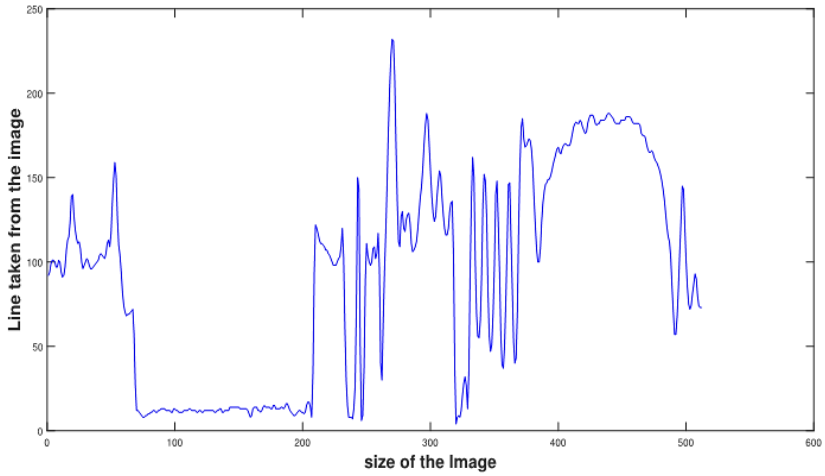

(a) True signal

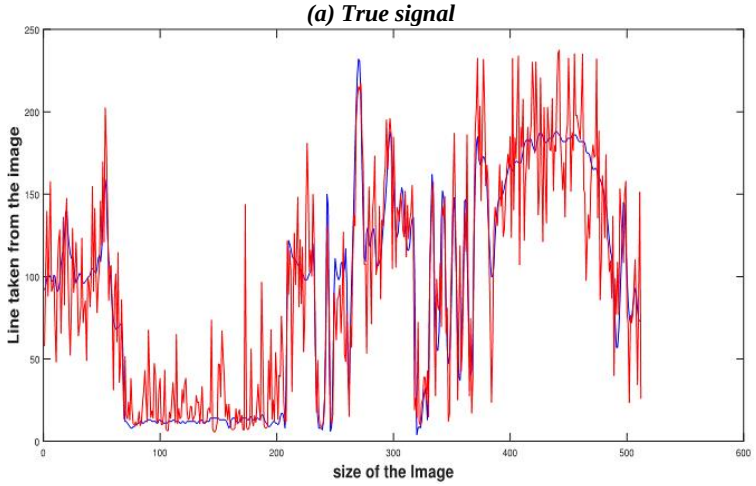

(b) True and noise signals

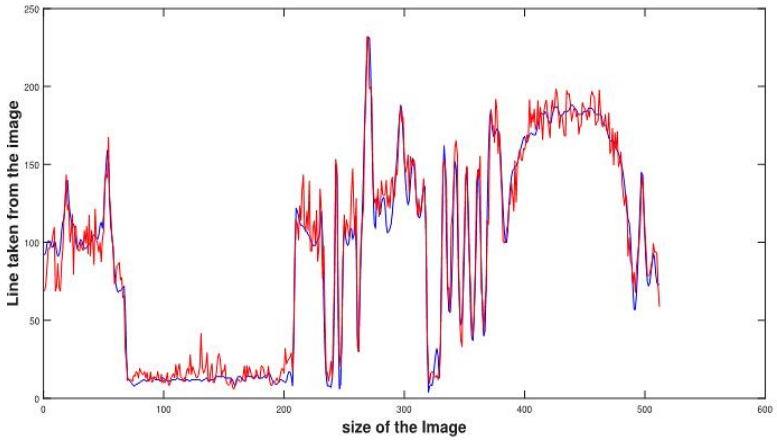

(c) M1

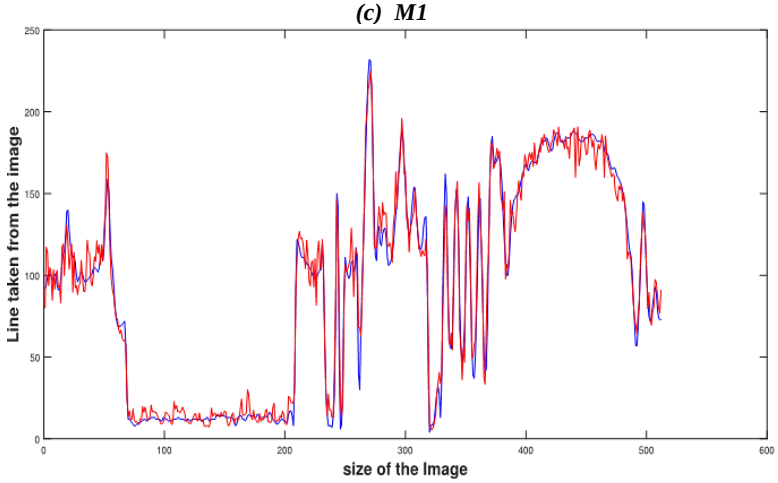

(d) M2 – IMQ

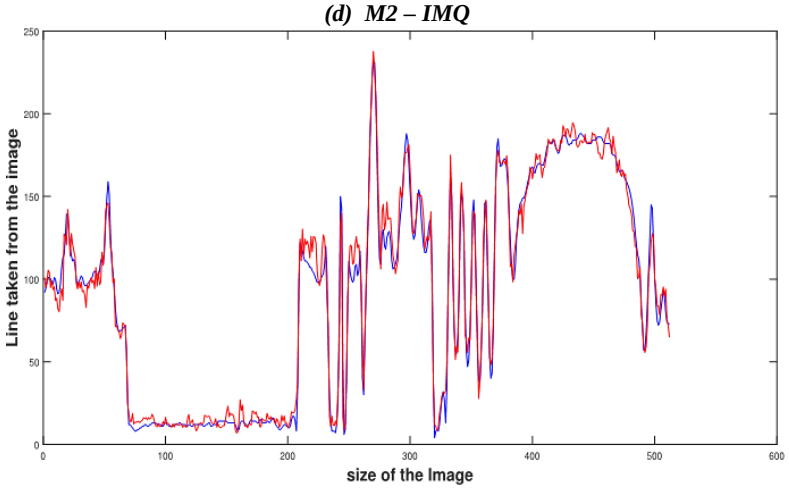

(e) M2-GA

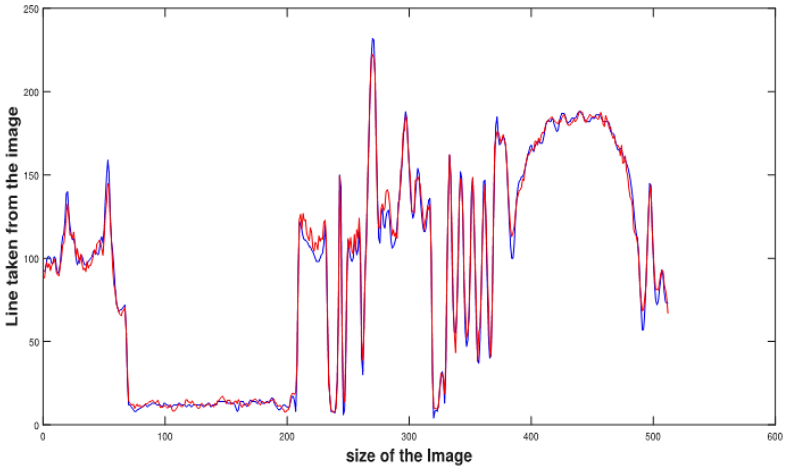

(f) M2 - MQ

Figure 3: Compassion of original and noisy signals taken from Lena image connected with salt and pepper noise $L2 = 38\%$, these are denoted by (a) and (b); original and restored signals by using M1 and M2 for IMQ-RBF, GA-RBF, and MQ-RBF, respectively. These signals are shown in (c), (d), (e), and (f), respectively. Here the blue line indicates the original signal whereas the red line indicates the noisy or restored signal. The Selected values of involved parameters are $c = 1.25$and $\lambda = 13$.

Experiment 4

In this examination, we conducted a comparison between the localized meshless scheme M2 and the Global Collection scheme (GMS) M3, as well as the traditional mesh-based scheme M1, for signal restoration with additive Gaussian noise $L1 = 30\%$. The true and noisy signals can be seen in Figures 4(a) and 4(b). The Local meshless scheme M2, which selects center points based on stencil points around a particular center point, is a more systematic approach compared to the Global meshless scheme M3 [19, 20]. Due to this distinction, the Local meshless scheme M2 outperforms the GMS M3 in signal restoration. Both the Local and Global schemes M2 and M3 use the same number of center values, p=60. The localized meshless method M2 demonstrated superior and faster restoration performance compared to M3 and M1 due to its meshless application. These signals are depicted in Figures 4(c), 4(d), 4(e), 4(f), and Table 6. Additionally, the global method, being a meshless scheme, results in better performance than the traditional mesh-based method M1 due to its meshless nature and simple implementation. These results are presented in Fig 4. Overall, the Local meshless scheme's more systematic approach to center point selection makes it superior to the GMS M3 in signal restoration.

The main limitation in our work is the selection of optimal values of parameters involved in the proposed Local Meshless schemes (LMS) hard to select by "head and trail" rules and also time-consuming.

Table 6: Comparison of SNR values of M1, M3, and M2 regarding SNR values.

S.No.	Signal selected of the Image	Size	SNR		
			M1	GMS-M3	Proposed scheme- M2
1	90th	512th	24.19	24.70	24.87

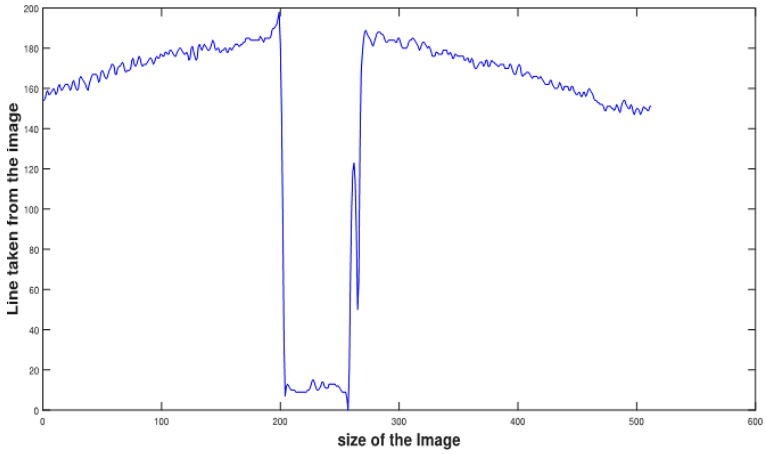

(a) True signal

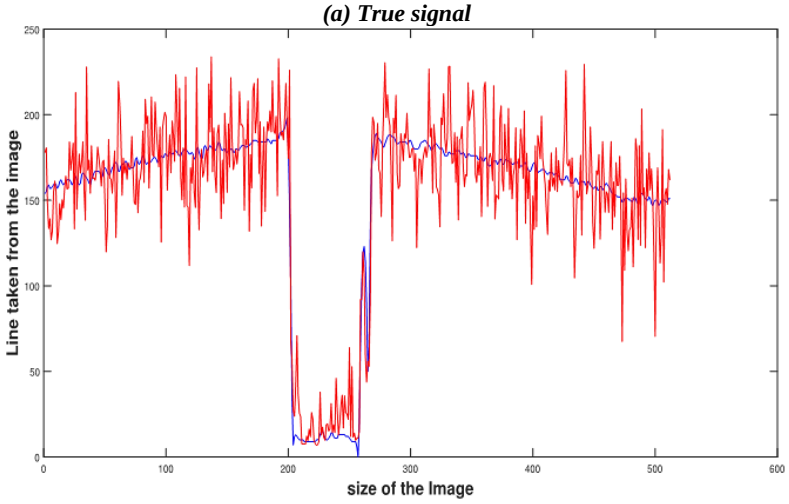

(b) True and noise signals

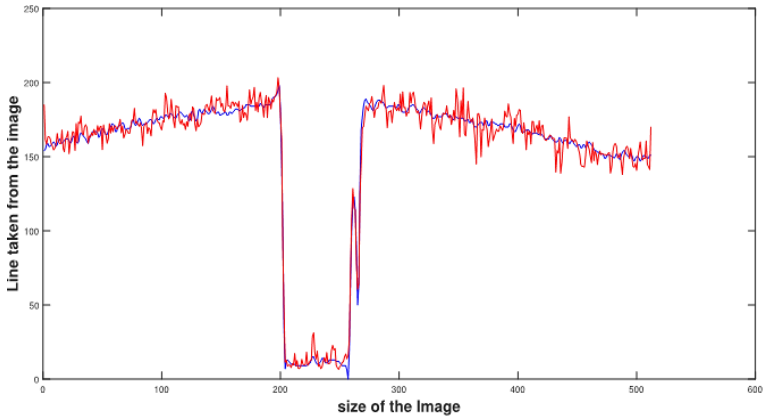

(c) M1

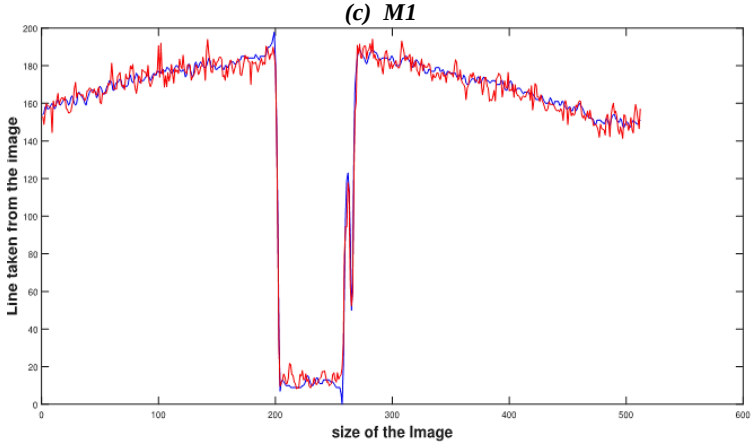

(d) M3 – GMS

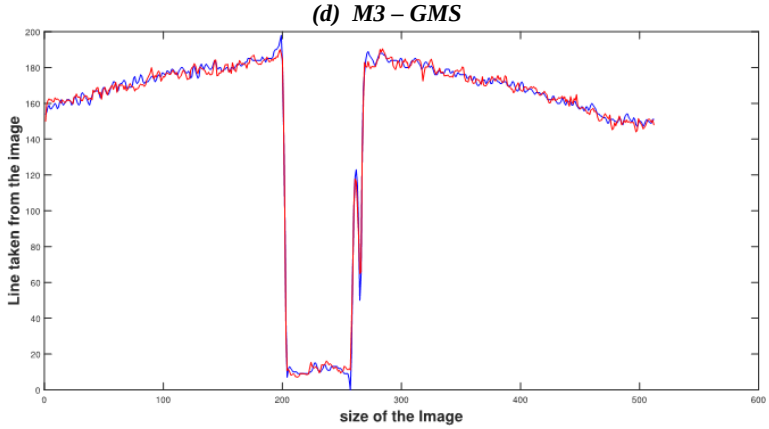

(e) M2 – Proposed method

Figure 4: (a) and (b) represent the true and noisy image with additive Gaussian noise $L1 = 30\%$. While (c), (d), and (e) indicate respectively the obtained lines using M1, GMS M3, and proposed method M2. Here the blue

line indicates the original signal whereas the red line indicates the noisy or restored signal. The values of the parameters are $c = 1.26$ ***and*** $\lambda = 14$.

Conclusion

In this article, Local Collocation Scheme (LMS) has been introduced to solve the associated Euler Lagrange PED connected with ROF model. Due to the local meshless applications and Multi-Quadric Radial Basis Function (MQ-RBF), this scheme is helpful to get the smooth solution regarding signal restoration. The experimental outcomes reveal that the Local meshless method is not only produce better restoration performance than traditional scheme regarding signal restoration (SNR) but also faster restoration outcomes. The Local Meshless Algorithm is also not only producing better restoration for MQ-RBF than IMQ-RBF and GA-RBF but also generates better restoration outcomes than Global RBF method for same MQ-RBF as basis function.

However, the optimal values of parameters involved in the meshless shape parameter hard to select. This limitation is under consideration and will be addressed in the subsequent paper.

Appendix

The following are the derivatives utilized in Equation (34) using the Local Meshless technique M2: Given that Equation (29) is

$$p = H^{-1}v_0, \tag{40}$$

After performing RBF interpolation and evaluating the derivative at N evaluation points $\left(\{x_i\}_{i=1}^{N}\right)$ and N_c center points$\left(\{x_j\}_{j=1}^{N}\right)$, we obtain

$$v(x) = \sum_{i=1}^{N} pj\varphi\left(\left\|x_i - xc_j\right\|_2\right), \tag{41}$$

Or

$$v = Hp, \tag{42}$$

where $N \times N_C$ is evaluated by matrix H, that is,

$$K = [\varphi_{ij}] = \left[\left(\left\|x_i - xc_j\right\|_2\right)\right], \tag{43}$$

$$for i = 1,2,3,\ldots\ldots N, j = 1,2,3,\ldots\ldots N_C,$$

The derivative from (34) then appears as under.

$$\frac{\partial v}{\partial x_i} = \sum_{j=1}^{N_C} p_j \frac{\partial}{\partial x_i}\varphi\left(\left\|x_i - x_j\right\|_2\right), \tag{44}$$

or

$$\frac{\partial v}{\partial x_i} = \frac{\partial}{\partial x_i}Kp. \tag{45}$$

Where

$$\frac{\partial h}{\partial x_i} = \frac{\partial [\varphi_{ij}]}{\partial x_i} = \frac{\partial}{\partial x_i}[\varphi(\|x_i - xc_j\|)], \tag{46}$$

$for i = 1,2,3,\ldots..N, j = 1,2,3,\ldots..N_C$

Combining Equations (34) and (42) we have

$$\frac{\partial v}{\partial x_i} = \frac{\partial}{\partial x_i} KH^{-1} v_0. \tag{47}$$

Define $M = KH^{-1}$, then above Equation (47) can be rewrite as

$$\frac{\partial v}{\partial x_i} = \frac{\partial}{\partial x_i} Mv_0 = M_{x_i} v_0. \tag{48}$$

The differentiation matrix can be define as

$$M_{x_i} = \frac{\partial}{\partial x_i} KH^{-1} = K_{x_i} H^{-1}. \tag{49}$$

For second derivative, we have

$$M_{x_i x_i} = \frac{\partial^2}{\partial x_i^2} KH^{-1} = K_{x_i x_i} H^{-1}. \tag{50}$$

Also

$$\frac{\partial^2 v}{\partial x_i^2} = \frac{\partial^2}{\partial x_i^2} Mv_0 = M_{x_i x_i} v_0. \tag{51}$$

Given that the system matrix H is known to be invertible, the differentiation matrix is clearly defined.

The chain rule provides $\varphi[r(x)]$, for every substantially differentiable RBF.

$$\frac{\partial \varphi}{\partial x_i} = \frac{d\varphi}{dr} \frac{\partial r}{\partial x_i}. \tag{52}$$

Regarding the initial derivative, having

$$\frac{\partial r}{\partial x_i} = \frac{x_i}{r}. \tag{53}$$

The calculation for the second derivative is as follows:

$$\frac{\partial^2 \varphi}{\partial x_i} = \frac{d\varphi}{dr} \frac{\partial^2 r}{\partial x_i^2} + \frac{d^2 \varphi}{dr^2} \left(\frac{\partial r}{\partial x_i}\right)^2, \tag{54}$$

With

$$\frac{\partial^2 r}{\partial x_i^2} = \frac{1 - \left[\frac{\partial r}{\partial x_i}\right]^2}{r}. \tag{55}$$

Specifically for the MQ,

$$\frac{d\varphi}{dr} = \frac{d[c^2 + r^2]^{\frac{1}{2}}}{dr} = \frac{r}{[c^2 + r^2]^{\frac{1}{2}}}, \tag{56}$$

And

$$\frac{d\varphi}{dr^2} = \frac{c^2}{[c^2 + r^2]^{\frac{3}{2}}}. \tag{57}$$

References

Bai, J., & Feng, X. C. (2018). Image denoising using generalized anisotropic diffusion. *Journal of Mathematical Imaging and Vision*, *60*, 994-1007.

Chambolle, A., Caselles, V., Cremers, D., Novaga, M., & Pock, T. (2010). An introduction to total variation for image analysis. *Theoretical foundations and numerical methods for sparse recovery*, *9*(263 340), 227.

Chan, T., Esedoglu, S., Park, F., & Yip, A. (2006). Total variation image restoration: Overview and recent developments. *Handbook of mathematical models in computer vision*, 17-31.

Chang, Q., Tai, X. C., & Xing, L. (2009). A compound algorithm of denoising using second-order and fourth-order partial differential equations. *Numer. Math. Theory Methods Appl*, *2*, 353-376.

Chenoweth, M. E. (2012). A local radial basis function method for the numerical solution of partial differential equations.

Doha, E. H., Baleanu, D., Bhrawy, A. H., & Abdelkawy, M. A. (2013). A Jacobi Collocation Method for Solving Nonlinear Burgers-Type equations. In *Abstract and Applied Analysis* (Vol. 2013, No. 1, p. 760542). Hindawi Publishing Corporation.

Eslahchi, M. R., Dehghan, M., & Parvizi, M. (2014). Application of the collocation method for solving nonlinear fractional integro differential equations. *Journal of Computational and Applied Mathematics*, *257*, 105-128.

Guo, L., Chen, W., Liao, Y., Liao, H., & Li, J. (2016). An Edge-Preserved Image Denoising Algorithm Based on Local Adaptive Regularization. *Journal of Sensors*, *2016*(1), 2019569.

Hosseini, B., & Hashemi, R. (2011). Solution of Burgers' equation using a local-RBF meshless method. *International Journal for Computational Methods in Engineering Science and Mechanics*, *12*(1), 44-58.

Houstis, E. (1978). A collocation method for systems of nonlinear ordinary differential equations. *Journal of Mathematical Analysis and Applications*, *62*(1), 24-37.

Jankowska, M. A., Karageorghis, A., & Chen, C. S. (2018). Kansa RBF method for nonlinear problems. *Boundary Elements and Other Mesh Reduction Methods*, *39*.

Jiang, D. H., Tan, X., Liang, Y. Q., & Fang, S. (2015). A new nonlocal variational bi-regularized image restoration model via split

Bregman method. *EURASIP Journal on Image and Video Processing*, *2015*, 1-10.

Jiang, Y., & Zhang, S. L. (2013). Image Denoising Based on the Modified ROF Model.

Kansa, E. J. (1990). Multiquadrics—A scattered data approximation scheme with applications to computational fluid-dynamics—I surface approximations and partial derivative estimates. *Computers & Mathematics with applications*, *19*(8-9), 127-145.

Kansa, E. J. (1990). Multiquadrics—A scattered data approximation scheme with applications to computational fluid-dynamics—II solutions to parabolic, hyperbolic and elliptic partial differential equations. *Computers & mathematics with applications*, *19*(8-9), 147-161.

Kansa, E. J. (1990). Multiquadrics—A scattered data approximation scheme with applications to computational fluid-dynamics—II solutions to parabolic, hyperbolic and elliptic partial differential equations. *Computers & mathematics with applications*, *19*(8-9), 147-161.

Kansa, E. J. (1999). Motivation for using radial basis functions to solve PDEs. *RN*, *64*(1), 1.

Kervrann, C. (2004). An adaptive window approach for image smoothing and structures preserving. In *Computer Vision-ECCV 2004: 8th European Conference on Computer Vision, Prague, Czech Republic, May 11-14, 2004. Proceedings, Part III 8* (pp. 132-144). Springer Berlin Heidelberg.

Khan, M. A., Chen, W., Ullah, A., & Fu, Z. (2017). A mesh-free algorithm for ROF model. *EURASIP Journal on Advances in Signal Processing*, *2017*, 1-16.

Krishnan, D., Lin, P., & Tai, X. C. (2006). An efficient operator splitting method for noise removal in images. *Commun. Comput. Phys*, *1*(5), 847-858.

Larsson, E., & Fornberg, B. (2003). A numerical study of some radial basis function based solution methods for elliptic PDEs. *Computers & Mathematics with Applications*, *46*(5-6), 891-902.

Levesley, J. (2004). Radial Basis Functions: Theory and Implementations.

Li, J., Cheng, A. H. D., & Chen, C. S. (2003). A comparison of efficiency and error convergence of multiquadric collocation method and finite element method. *Engineering Analysis with Boundary Elements*, *27*(3), 251-257.

Li, X., Li, L., & Wang, Q. H. (2018). Wavelet-based iterative perfect reconstruction in computational integral imaging. *JOSA A*, *35*(7), 1212-1220.

Luo, L., Zhao, Z. Q., Li, X. P., & Feng, X. C. (2019). A stochastic image denoising method based on adaptive patch-size. *Multidimensional Systems and Signal Processing*, *30*, 705-725.

Lysaker, M., Lundervold, A., & Tai, X. C. (2003). Noise removal using fourth-order partial differential equation with applications to medical magnetic resonance images in space and time. *IEEE Transactions on image processing*, *12*(12), 1579-1590.

Lysaker, M., Osher, S., & Tai, X. C. (2004). Noise removal using smoothed normals and surface fitting. *IEEE Transactions on image processing*, *13*(10), 1345-1357.

Madych, W. R., & Nelson, S. A. (1983). Multivariate interpolation: a variational theory.

Micchelli, C. A. (1984). *Interpolation of scattered data: distance matrices and conditionally positive definite functions* (pp. 143-145). Springer Netherlands.

Naveed, K., Shaukat, B., Ehsan, S., Mcdonald-Maier, K. D., & Ur Rehman, N. (2019). Multiscale image denoising using goodness of-fit test based on EDF statistics. *PLoS One*, *14*(5), e0216197.

Ordokhani, Y., & Razzaghi, M. (2008). Solution of nonlinear Volterra Fredholm–Hammerstein integral equations via a collocation method and rationalized Haar functions. *Applied Mathematics Letters*, *21*(1), 4-9.

Osher, S., Burger, M., Goldfarb, D., Xu, J., & Yin, W. (2005). An iterative regularization method for total variation-based image restoration. *Multiscale Modeling & Simulation*, *4*(2), 460-489.

Parand, K., & Rad, J. A. (2012). Numerical solution of nonlinear Volterra Fredholm–Hammerstein integral equations via collocation method based on radial basis functions. *Applied Mathematics and Computation*, *218*(9), 5292-5309.

Polzehl, J., & Tabelow, K. (2007). Adaptive smoothing of digital images: The R package adimpro.

Ramadhan, A., Mahmood, F., & Elci, A. (2017). Image denoising by median filter in wavelet domain. *arXiv preprint arXiv:1703.06499*.

Rudin, L. I., & Osher, S. (1994, November). Total variation based image restoration with free local constraints. In *Proceedings of 1st international conference on image processing* (Vol. 1, pp. 31-35). IEEE.

Rudin, L. I., Osher, S., & Fatemi, E. (1992). Nonlinear total variation based noise removal algorithms. *Physica D: nonlinear phenomena*, *60*(1-4), 259-268.

Satapathy, L. M., Das, P., Shatapathy, A., & Patel, A. K. (2019). Bio medical image denoising using wavelet transform. *Int. J. Recent Technol. Eng*, *8*(1), 2874-2879.

Sarra, S. A. (2011). Radial basis function approximation methods with extended precision floating point arithmetic. *Engineering Analysis with Boundary Elements*, *35*(1), 68-76.

Sarra, S. A. (2012). A local radial basis function method for advection diffusion–reaction equations on complexly shaped domains. *Applied mathematics and Computation*, *218*(19), 9853 9865.

Shen, Q. (2011). Numerical solution of the Sturm–Liouville problem with local RBF-based differential quadrature collocation method. *International Journal of Computer Mathematics*, *88*(2), 285-295.

Shan, Y. Y., Shu, C., & Qin, N. (2009). Multiquadric finite difference (MQ-FD) method and its application. *Adv. Appl. Math. Mech*, *1*(5), 615-638.

Zerroukat, M., Power, H., & Chen, C. (1998). A numerical method for heat transfer problems using collocation and radial basis functions. *International Journal for numerical methods in Engineering*, *42*(7), 1263-1278.